




Essential role of papillae flexibility in nectar capture by bees

Amandine Lechantre^{a,b,c,1,2} , Ayrton Draux^{a,2}, Hoa-Ai Béatrice Hua^d , Denis Michez^e , Pascal Damman^a , and Fabian Brau^{d,3} 

^aLaboratoire Interfaces & Fluides Complexes, Université de Mons, B-7000 Mons, Belgium; ^bLaboratoire de Physique et Mécanique des Milieux Hétérogènes (PMMH), UMR 7636 of CNRS, École Supérieure de Physique et de Chimie Industrielles, 75005 Paris, France; ^cLaboratoire Matières et Systèmes Complexes (MSC), UMR 7057 of CNRS, Université de Paris, 75006 Paris, France; ^dNonlinear Physical Chemistry Unit, Université libre de Bruxelles, 1050 Bruxelles, Belgium; and ^eLaboratoire de Zoologie, Université de Mons, B-7000 Mons, Belgium

Edited by David A. Weitz, Harvard University, Cambridge, MA, and approved March 28, 2021 (received for review December 11, 2020)

Many bees possess a tongue resembling a brush composed of a central rod (glossa) covered by elongated papillae, which is dipped periodically into nectar to collect this primary source of energy. In vivo measurements show that the amount of nectar collected per lap remains essentially constant for sugar concentrations lower than 50% but drops significantly for a concentration around 70%. To understand this variation of the ingestion rate with the sugar content of nectar, we investigate the dynamics of fluid capture by *Bombus terrestris* as a model system. During the dipping process, the papillae, which initially adhere to the glossa, unfold when immersed in the nectar. Combining in vivo investigations, macroscopic experiments with flexible rods, and an elastoviscous theoretical model, we show that the capture mechanism is governed by the relaxation dynamics of the bent papillae, driven by their elastic recoil slowed down through viscous dissipation. At low sugar concentrations, the papillae completely open before the tongue retracts out of nectar and thus, fully contribute to the fluid capture. In contrast, at larger concentrations corresponding to the drop of the ingestion rate, the viscous dissipation strongly hinders the papillae opening, reducing considerably the amount of nectar captured. This study shows the crucial role of flexible papillae, whose aspect ratio determines the optimal nectar concentration, to understand quantitatively the capture of nectar by bees and how physics can shed some light on the degree of adaptation of a specific morphological trait.

bee | nectar capture | fluid–structure interaction | viscous dissipation

The ingestion of liquids to stay hydrated is an essential need for living organisms. Various natural strategies have emerged during the course of evolution to transport fluids. Large animals typically use gravity to drink low-viscosity fluids like water (human, birds) or use various methods to counteract gravity such as lapping [feline (1)], lading [Canidae (2)], or active suction (Bovidae, Equidae). Small animals use instead viscous and capillary suction (butterflies, hummingbirds, etc.), dipping (bees, ants, bats, etc.), or contrasted wetting properties of their body (Namib desert beetle) to capture fluids (3, 4).

Some insects, birds, and small mammals hydrate and feed simultaneously by ingesting nectar. Capturing such a viscous fluid at small scales is a challenge that nectarivores have solved by developing various types of specialized tongues through natural selection leading to the propagation of favorable traits (5). The coevolution of bees and flowers is a well-known example of such mechanisms highlighted by the various shapes of the tongue observed among bee species in relation to the diversity in flower morphology (6). One intuitive example is the correlation between the corolla depth and the tongue length (7–10).

The relation between the nectar sugar concentration and the bees' tongue morphology is more subtle. Indeed, since the energy content of a given volume of nectar is proportional to its sugar concentration, flowers should a priori produce the sweetest possible nectar to attract bees interested by maximizing their energy

intake. However, our in vivo measurements for *Bombus* show that very sweet nectar is not the best for bees. Fig. 1A shows images of a *Bombus terrestris* feeding on a sugar solution. The meniscus at the liquid–air interface moves in average at a constant speed, v_m , inside the capillary tube as the liquid is ingested by the *Bombus* and yields the ingestion rate $Q = v_m S_c$ where S_c is the area of the inner section of the capillary (Fig. 1B and *Materials and Methods*). The temporal evolution of the meniscus position $p(t)$ reveals, however, small periodic variations related to the periodic motion of the tongue from which the lapping rate T_L^{-1} is determined (Fig. 1B, *Inset*). Repeating this experiment at various sugar concentrations, c_s , shows that the lapping rate is essentially constant (Fig. 1C) with a lapping time $T_L \simeq 0.2$ s in agreement with previous measurements on various bee species (11–13, 15–18). For each concentration considered, the ingestion rate is obtained and reported in Fig. 1D together with others found in the literature for other bee species (11, 14). Those results show that the ingestion rate of nectar remains essentially constant for sugar concentrations $c_s \lesssim 50\%$ but decreases significantly at 70%. As shown below, this implies that the energy intake rate is maximum around $c_s^* \simeq 50$ to 60%. Therefore, there is no reason for plants visited by bees to produce nectar with $c_s > c_s^*$. This may explain why the sugar concentration of flower nectar rarely exceeds 60% (25, 26).

Significance

Flowers provide the energy resources of bees. In a competitive world, we can hypothesize that flowers attract bees by producing very sweet nectar since it offers the greatest energetic rewards. However, the nectar sugar concentration rarely exceed 60%, and in vivo measurements show that bees capture nectar less efficiently beyond that limit. Here, we explain the physiological origin of this limit based on an elastoviscous mechanism. Most of bees collect the nectar with tongues covered by elongated papillae that open when immersed in a fluid, the opening dynamics determining the amount of nectar collected per lap. At very large sugar concentrations, we found that viscous forces impede the full opening of papillae, reducing the amount of nectar collected.

Author contributions: D.M., P.D., and F.B. designed research; A.L., A.D., H.-A.B.H., and F.B. performed research; A.D. and F.B. analyzed data; and P.D. and F.B. wrote the paper.

The authors declare no competing interest.

This article is a PNAS Direct Submission.

Published under the PNAS license.

¹ Present address: Institut de Physique de Nice, Université Nice Côte d'Azur, CNRS-UMR 7010, 06100 Nice, France.

² A.L. and A.D. contributed equally to this work.

³ To whom correspondence may be addressed. Email: fabian.brau@ulb.be.

This article contains supporting information online at <https://www.pnas.org/lookup/suppl/doi:10.1073/pnas.2025513118/-DCSupplemental>.

Published April 30, 2021.

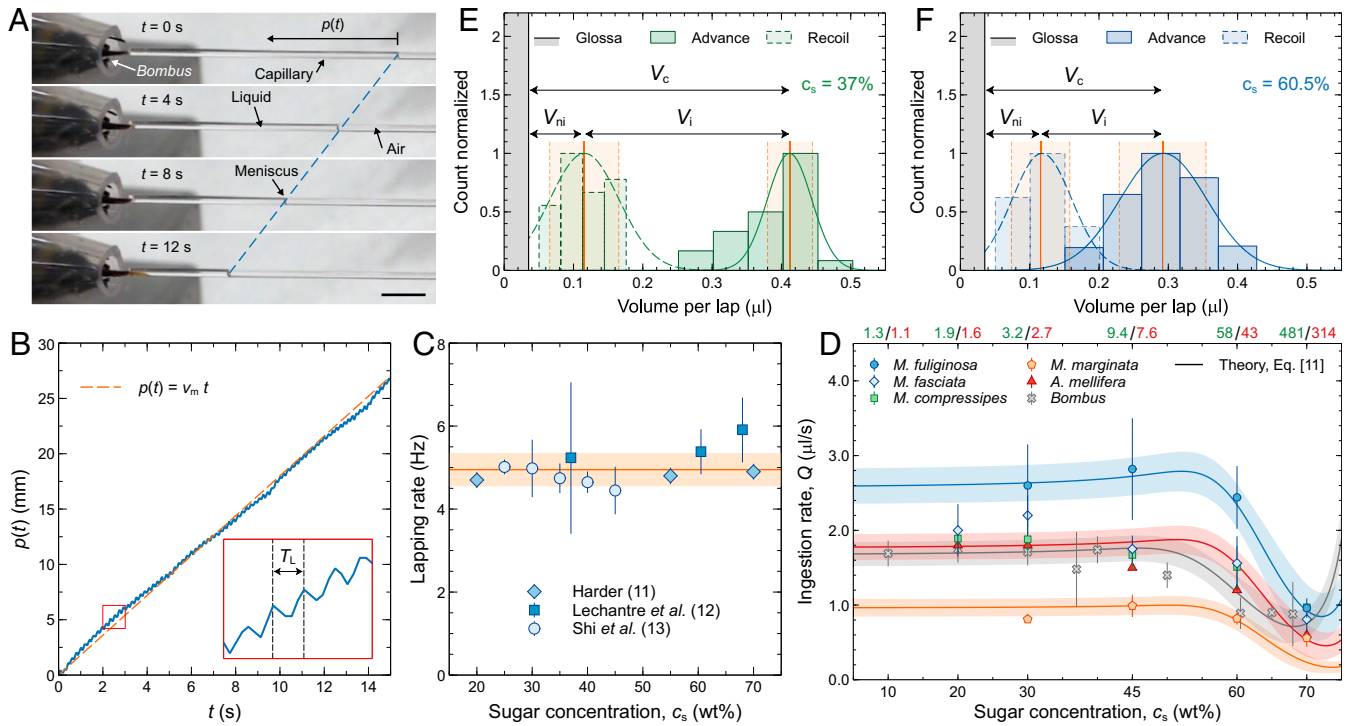


Fig. 1. (A) Snapshots of a feeding process with a 60.5% sugar solution ($\mu = 0.065$ Pa s) (Movie S1). (Scale bar: 5 mm.) (B) Evolution of the position $p(t)$ of the liquid–air interface as a function of time during the feeding process shown in A. (Inset) Evolution of $p(t)$ between $t = 2$ s and $t = 3$ s. (C) Lapping rate as a function of the sugar concentration c_s at 20 °C (11–13). The shaded area highlights the range $T_L^{-1} = (4.95 \pm 0.40)$ Hz. (D) Comparison between the theoretical ingestion rate Q (Eq. 11) and in vivo measurements for different species of *Melipona*, *Apis* (14), and *Bombus* (11, 12) as a function of the sugar concentration. The viscosity in millipascals second at 20 °C/30 °C is also indicated on the top axis. The parameter values used are $T_L = 2T_R = (0.20 \pm 0.02)$ s (11–13, 15–18), $d_m = L \sin(\pi/4)$ (16, 18–20), and $E = (1.1 \pm 0.1)$ MPa for all species; $R_G = (50 \pm 5)$ μ m, $R = (2.9 \pm 0.1)$ μ m, and $L = (170 \pm 5)$ μ m (19, 21) for *Melipona* and *Apis*; and $R_G = (95 \pm 5)$ μ m, $R = (2.1 \pm 0.1)$ μ m, and $L = (135 \pm 5)$ μ m for *Bombus*. The value of E is comparable with the Young modulus of the tip of the adhesive tarsal setae of beetles (22, 23) or of the lepidopteran proboscis (24) (discussion is in SI Appendix). The small variation of the nectar density ρ_l with μ is negligible due to the small exponent in Eq. 10, and $\rho_l = (1,175 \pm 175)$ kg/m³ is used (SI Appendix). The immersion length, L_I , of the tongue is varied proportionally to the tongue length, L_T , for each species [$L_I \simeq (0.6 L_T - 1)$ mm]: $L_I = 3.2 \pm 0.1$ mm (*Melipona fuliginosa*, $L_T = 7.0$ mm), $L_I = 2.2 \pm 0.1$ mm (*Apis mellifera*, $L_T = 5.4$ mm), $L_I = 2.0 \pm 0.1$ mm (*Bombus*, $L_T = 5.0$ mm), and $L_I = 1.2 \pm 0.1$ mm (*Melipona marginata*, $L_T = 3.8$ mm) (12, 14). The theoretical curves for *Melipona fasciata* and *Melipona compressipes* ($L_T = 5.9$ mm) are close to the one for *A. mellifera* and are not shown for clarity. The shaded areas show the regions spanned by the theoretical curves when the parameters are varied within their error bars. (E and F) Distributions of the volumes per lap associated with the advances and recoils of the meniscus seen in B, Inset for $c_s = 37\%$ and 62 laps (E) and $c_s = 60.5\%$ and 261 laps (F). The distributions are fitted by normal distributions, and the orange shaded areas extend over one SD around the mean value.

Two origins can be considered to explain the drop in ingestion rate observed for a concentration near 70%. It could be related either to the difficulty to swallow nectar when its viscosity (c_s) increases or to an intrinsic limitation of the capture mechanisms itself (i.e., the tongue captures less nectar per lap as c_s increases). Interestingly, the small periodic oscillations of the meniscus position $p(t)$ seen in Fig. 1B allow us to discriminate between both explanations. As the tongue enters the liquid, the meniscus recoils due to the added extra volume composed of the tongue and the remaining noningested fluid (V_{ni}). When the tongue exits the capillary, in contrast, the meniscus advances due to the lost volume related to the tongue and the captured fluid (V_c) removed from the capillary. The amount of ingested nectar is then given by $V_i = V_c - V_{ni}$. The distributions of V_c and V_{ni} for two values of sugar concentration c_s are shown in Fig. 1E and F. Clearly, V_{ni} is insensitive to variations in c_s , whereas V_c decreases as c_s increases. These results indicate that the drop in the volume ingested per lap, V_i , is due to a decrease of the amount of nectar captured by the tongue when c_s increases.

The loss of efficiency of the bees' tongues in capturing very sweet nectar should then be related to its fine structure, which is ignored in previous models (27). The viscous dipping of smooth rods does not account for the drop in ingestion rate. Indeed, since the bees' lapping period, T_L , is essentially constant, the

thickness of the liquid layer covering a bare tongue when it retracts out of nectar should increase monotonically with its viscosity and thus, with its sugar concentration, according to the Landau–Levich–Derjaguin (LLD) mechanism (28–31).

The tongue of a bee is composed of a glossa of radius $R_G \sim (50 - 100)$ μ m decorated by solid elongated papillae of length $L \sim (100 - 200)$ μ m and radius $R \sim (2 - 3)$ μ m (12, 15–21, 32–35) (SI Appendix). There are approximately 2,500 papillae per square millimeter so that the average distance between them is about $8R$ (15, 17, 19, 21, 33, 34). This density is thus quite small compared with the setae density on the adhesive pads of some arthropods such as fly (*Calliphora erythrocephala*, $1.5 \times 10^5/\text{mm}^2$), bug (*Rhodnius*, $2 \times 10^5/\text{mm}^2$), or spider (*Cupiennius salei*, $2.1 \times 10^6/\text{mm}^2$) (36). During the drinking process, the papillae initially adhere to the glossa due to capillary forces and open when immersed in the nectar (Movie S1). Fig. 2A and B shows indeed that capillary forces are strong enough to keep the papillae bent in contact with the glossa. This elastocapillary effect is also observed when bees feed on dry sugar since the papillae open well after the protrusion phase and only when enough saliva is secreted to dissolve the sugar (37).

To determine the role of the papillae in the nectar capture, we analyze their in vivo dynamics recorded with an optical microscope fitted with a high-speed camera for *B. terrestris* (Materials

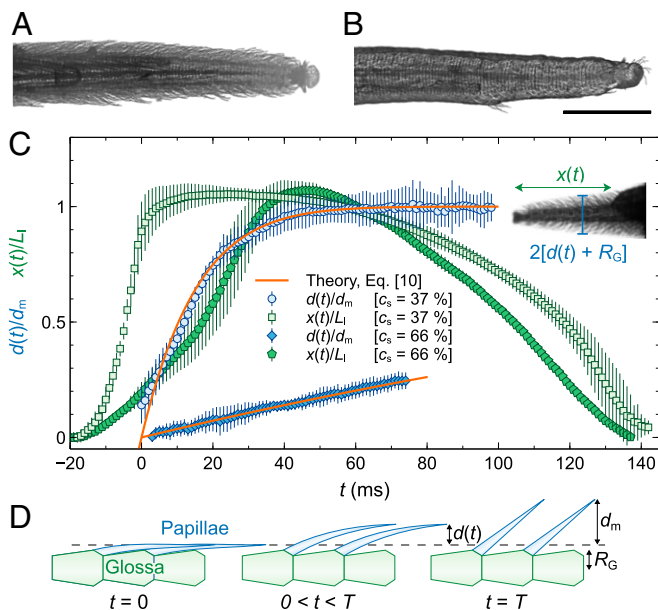


Fig. 2. (A and B) Optical microscopy photography of a *B. terrestris* tongue. The papillae are fully open when the tongue is immersed in water (A), whereas they adhere to the glossa due to capillary forces after the tongue is withdrawn from the liquid (B). (Scale bar: 500 μm .) (C) Evolution of the rescaled distances $x(t)/L_1$ and $d(t)/d_m$ as a function of time for two values of c_s for *B. terrestris*. $L_1 \simeq 2$ mm is the immersion length of the tongue, and $d_m \simeq 95$ μm is the maximum extension of the papillae. $d(t)$ is the average of measurements performed at four distances from the tip of the tongue (500, 750, 1,000, and 1,250 μm) (SI Appendix has raw data). The theoretical curves [10] are shown with $\rho_l = 1,150$ kg/m^3 , $\mu = 5$, and 200 mPa s (20°C) together with E , R , L , and d_m used in Fig. 1D for *Bombus*. (D) Schematic of the papillae relaxation dynamics.

and Methods). The temporal variations of the position of the tongue tip with respect to the galea, $x(t)$, and of the distance $d(t)$ between the tip of the papillae and the glossa during the capture process are shown in Fig. 2C. At low sugar concentration, c_s , the papillae open to reach a maximum extension $d_m \simeq 95$ μm before the tongue completely retracts out of the liquid and thus, fully contribute to the nectar capture. In contrast, at a larger c_s for which a drop of the ingestion rate is observed, the papillae do not have the time to completely open during a protraction–retraction cycle due to the viscous dissipation impacting both their dynamics and their benefits in collecting nectar. The temporal evolution of $x(t)$ shows that the protraction of the tongue is impacted by the nectar viscosity. However, in both cases shown in Fig. 2C, the total immersion length of the tongue, $L_1 \simeq 2$ mm, and the retraction time, $T_R \simeq 0.1$ s, are similar in agreement with the observation that the lapping frequency is essentially insensitive to the nectar viscosity (11–13). These observations further confirm that bees are able to adjust the retraction force to the nectar viscosity (12).

To mimic the opening dynamics of a single papilla, we consider the unbending dynamics of a deflected flexible rod in a viscous fluid. A rod of length L , radius R , Young modulus E , and density ρ_s is clamped at one extremity and deflected at its free end while immersed in a liquid of viscosity μ and density ρ_l (Fig. 3A and Materials and Methods). By varying systematically these control parameters, we show the existence of two regimes: under- and overdamped, separated by a transient stage. Each regime is characterized by distinct scaling for their relaxation times, T , defined as the time at which the rod passes through its rest position for the first time (Fig. 3B). For the underdamped regime, where the rod oscillates around its equilibrium position, T is pro-

portional to the oscillation period, whereas in the overdamped regime, there is no oscillation, and T is the time needed for the rod to return to equilibrium.

The theoretical analysis of the rod relaxation dynamics requires to couple the Navier–Stokes and elasticity equations and is unfortunately intractable. Therefore, we propose to decouple the fluid and the rod equations by adding an effective viscous force to the dynamical beam equation (38), which then reads

$$\bar{\rho}_{sl} \partial_t^2 w(x, t) = -B \partial_x^4 w(x, t) - F_\mu, \quad [1]$$

where $w(x, t)$ is the transverse displacement of the rod along the y axis, $B = \pi ER^4/4$ is the bending modulus of a cylindrical rod, $\bar{\rho}_{sl} = (\rho_s + \rho_l)S \equiv \rho_{sl}S$ is the linear mass density of the rod supplemented by the linear mass of the displaced fluid (39), and $S = \pi R^2$ is the section area of the rod.

The expression of the viscous force per unit length, F_μ , is a priori complicated since it depends on the local fluid velocity, which varies in space and time. Here, we propose to use the viscous drag experienced by a rigid cylinder moving at a constant speed perpendicular to its symmetry axis and obtained by solving the Stokes equations with the Oseen’s correction (40):

$$F_\mu = S_g \frac{4\pi\mu v}{c - \ln(v/v_c)}, \quad v_c = \frac{4\mu}{\rho_l R}, \quad [2]$$

where $v = |\partial_t w|$ is the rod velocity, S_g is the sign of $\partial_t w$ so that the viscous force is always acting against the rod motion, and $c = 1/2 - \gamma_E$ where $\gamma_E \simeq 0.577$ is the Euler constant. Notice that the data reported in Figs. 1D, 2C, and 3B are obtained with Newtonian fluids [at least up to $c_s = 85\%$ for sucrose solutions (41–43)].

Since Eqs. 1 and 2 depend on numerous parameters, it is useful to consider its adimensionalized form. Using $\bar{w} = w/\ell$, $\bar{x} = x/L$, and $\bar{t} = t/\tau$, where τ and ℓ are defined as

$$\tau = \rho_{sl} R^2 / 4\mu \quad \text{and} \quad \ell = v_c \tau, \quad [3]$$

we obtain the adimensionalized form of Eq. 1:

$$\partial_{\bar{t}}^2 \bar{w}(\bar{x}, \bar{t}) = -k \partial_{\bar{x}}^4 \bar{w}(\bar{x}, \bar{t}) - \bar{F}_\mu, \quad k = \frac{E \rho_{sl} R^6}{64 \mu^2 L^4}, \quad [4]$$

where $\bar{F}_\mu = S_g \bar{v} / [c - \ln \bar{v}]$ and $\bar{v} = v/v_c = |\partial_{\bar{t}} \bar{w}|$. Eq. 4 can be solved numerically by imposing that the deflected rod is clamped at $\bar{x} = 0$, free at $\bar{x} = 1$, and released without initial velocity as in the experiments. The relaxation times, T/τ , obtained from the numerical solutions are in good agreement with the experimental data spanning 12 orders of magnitude for k (Fig. 3B).

The relaxation dynamics of the bee’s papillae occur at low values of the ratio v/v_c , vide infra. To gain some analytical insights into the relaxation dynamics in this regime, we notice that, when $v/v_c \lesssim 10^{-3}$, the evolution of \bar{F}_μ with the velocity is described in very good approximation by a power law (Fig. 3C):

$$\bar{F}_\mu = S_g \beta \bar{v}^{11/10}, \quad \beta = 0.288. \quad [5]$$

The viscous force is thus not proportional to the rod velocity in agreement with the observed nonexponential relaxation dynamics reported in Fig. 3D. Notice, however, that to describe the evolution of the ingestion rate as a function of the sugar concentration shown in Fig. 1D, a linear approximation for the viscous force could also be used. The difference between the two descriptions is smaller than the typical uncertainty on the in vivo data (SI Appendix).

In the overdamped regime, the rod inertia is negligible, and since there is no oscillation, the rod velocity is negative such that

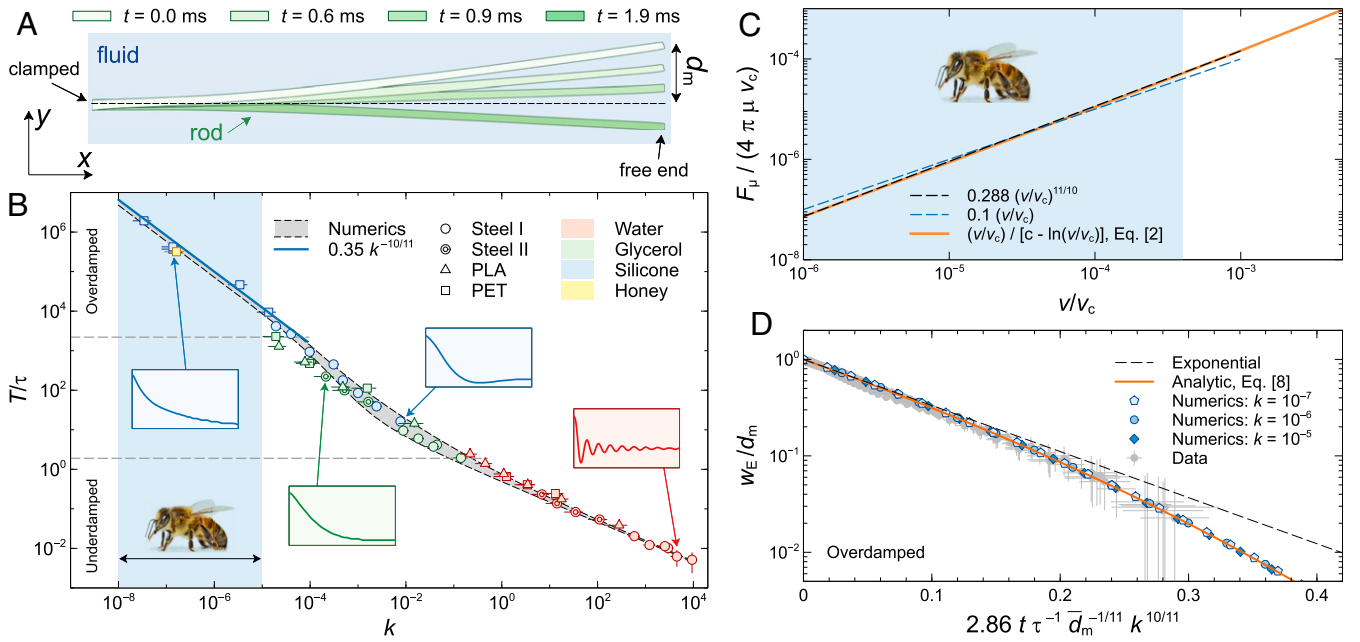


Fig. 3. (A) Snapshots of a deflected stainless steel rod of length $L = 54$ mm oscillating in water at various times as indicated. The horizontal dashed line indicates the equilibrium position. (B) Evolution of the experimental rescaled relaxation time T/τ as a function of the control parameter k (Eq. 4) for various types of rods and fluids. The gray shaded area shows the variation of the theoretical curve, obtained by solving numerically Eq. 4, as the rescaled imposed transverse displacement of the tip of the rod, \bar{d}_m , is varied within its experimental range ($0.4 \leq \bar{d}_m \leq 10.5$). (Insets) Positions of the tip of the rod as a function of time for some representative cases. (C) Evolution of the rescaled viscous force, $\bar{F}_\mu = F_\mu / (4\pi\mu v_c)$ (Eq. 2), as a function of the rescaled velocity, $\bar{v} = v/v_c$ (solid orange curve) together with a power law approximation for $\bar{v} \leq 10^{-3}$ (dashed black curve). (D) Evolution of the rescaled position of the tip of the rod, w_E/d_m , as a function of a rescaled time for the overdamped regime. Data obtained by solving numerically Eqs. 4 and 5 are compared with the experimental data and the asymptotic theoretical curve [8]. An exponential decay arising from a viscous force varying linearly with v is shown for comparison.

$|\partial_{\bar{t}} \bar{w}| = -\partial_{\bar{t}} \bar{w}$ and $S_g = -1$. Therefore, Eq. 4 with the viscous force [5] becomes

$$k \partial_{\bar{x}}^4 \bar{w}(\bar{x}, \bar{t}) = \beta [-\partial_{\bar{t}} \bar{w}(\bar{x}, \bar{t})]^{11/10}. \quad [6]$$

Using the separation of variables, $\bar{w}(\bar{x}, \bar{t}) = \bar{w}_E(\bar{t})g(\bar{x})$ where $\bar{w}_E(\bar{t})$ describes the temporal evolution of the tip of the rod, Eq. 6 reduces to two ordinary differential equations:

$$\dot{\bar{w}}_E = -[\eta k/\beta]^{10/11} \bar{w}_E^{10/11}, \quad \bar{w}_E(0) = \bar{d}_m, \quad [7a]$$

$$g'''' = \eta g^{11/10}, \quad g(0) = g'(0) = g''(1) = g'''(1) = 0, \quad [7b]$$

where η is the separation constant, $d_m = \ell \bar{d}_m$ is the imposed transverse displacement of the tip of the rod, and dot and prime indicate time and spatial derivatives, respectively. The boundary conditions indicate that the rod is clamped at $\bar{x} = 0$ and free at $\bar{x} = 1$ (Fig. 3A). The nonlinear eigenvalue Eq. 7b can be solved numerically with $g(1) = 1$ [i.e., $\bar{w}(1, 0) = \bar{d}_m$], so that $\eta \simeq 12.803$. The temporal evolution of the position of the tip of the rod is then obtained by integrating Eq. 7a:

$$\frac{\bar{w}_E(\bar{t})}{\bar{d}_m} = \left[1 - 2.86 \frac{k^{10/11}}{\bar{d}_m^{1/11}} \bar{t} \right]^{11}. \quad [8]$$

Fig. 3D shows that, when time is properly rescaled, the numerical solutions of Eqs. 4 and 5 at small k and the experimental data in overdamped regime collapse on the asymptotic expression [8]. The latter implies that the relaxation time T at which the rod returns to equilibrium (i.e., $w_E = 0$) is given by

$$T/\tau = 0.35 \bar{d}_m^{1/11} k^{-10/11} \simeq 0.35 k^{-10/11}. \quad [9]$$

Fig. 3B shows the good agreement between the asymptotic expression [9] and experimental data.

By measuring the relaxation time $T \gtrsim 0.06$ s of the papillae from in vivo measurements (Fig. 2C) (16, 19, 20), for $\mu = 5$ mPa s and using the radius R and the length L of the papillae reported in Fig. 1D, we find $v/v_c \simeq d_m/(v_c T) \lesssim 10^{-4}$ so that Eq. 5 is valid. Notice that, since $v/v_c \sim \mu^{-1}$, this ratio is even smaller at larger viscosity. The temporal evolution of the distance $d(t) = d_m - w_E(t)$ between the tip of the papillae and the glossa is thus obtained from Eq. 8:

$$\frac{d(t)}{d_m} = 1 - \left[1 - \frac{t}{T} \right]^{11}, \quad T = 4.35 \left[\frac{\mu^{10} d_m}{\bar{E}^{10} v_c} \right]^{1/11}, \quad [10]$$

where Eq. 9 has been written in a more convenient form with $\bar{E} = ER^4/L^4$ an effective rod stiffness. Eq. 10 describes the relaxation dynamics of the papillae as shown schematically in Fig. 2D. At $t = 0$, $d(0) = 0$, and the papillae adhere to the glossa; at $t = T$, $d(T) = d_m$, and the papillae are fully open. Using the parameter values reported in Fig. 1D for *Bombus*, the temporal evolution of $d(t)/d_m$ is found to be in very good quantitative agreement with in vivo measurements of the papillae relaxation dynamics (Fig. 2C).

A model for the nectar capture by bees taking into account the relaxation dynamics of the papillae can now be developed. Since the distance between the papillae is large compared with their radius ($\sim 8R$) and the Reynolds number is very low ($\text{Re} \sim v/v_c \lesssim 10^{-4}$), the interference between drag flows generated by adjacent papillae can be neglected (44, 45).

As shown in Fig. 1, bees collect nectar by quickly protracting and retracting their tongue with a constant lapping period, which is the sum of the protraction time, of the retraction time, and of the nectar unloading time. The volume of nectar collected when the tongue retracts out of nectar at $t = T_R \simeq T_L/2$ is the sum of

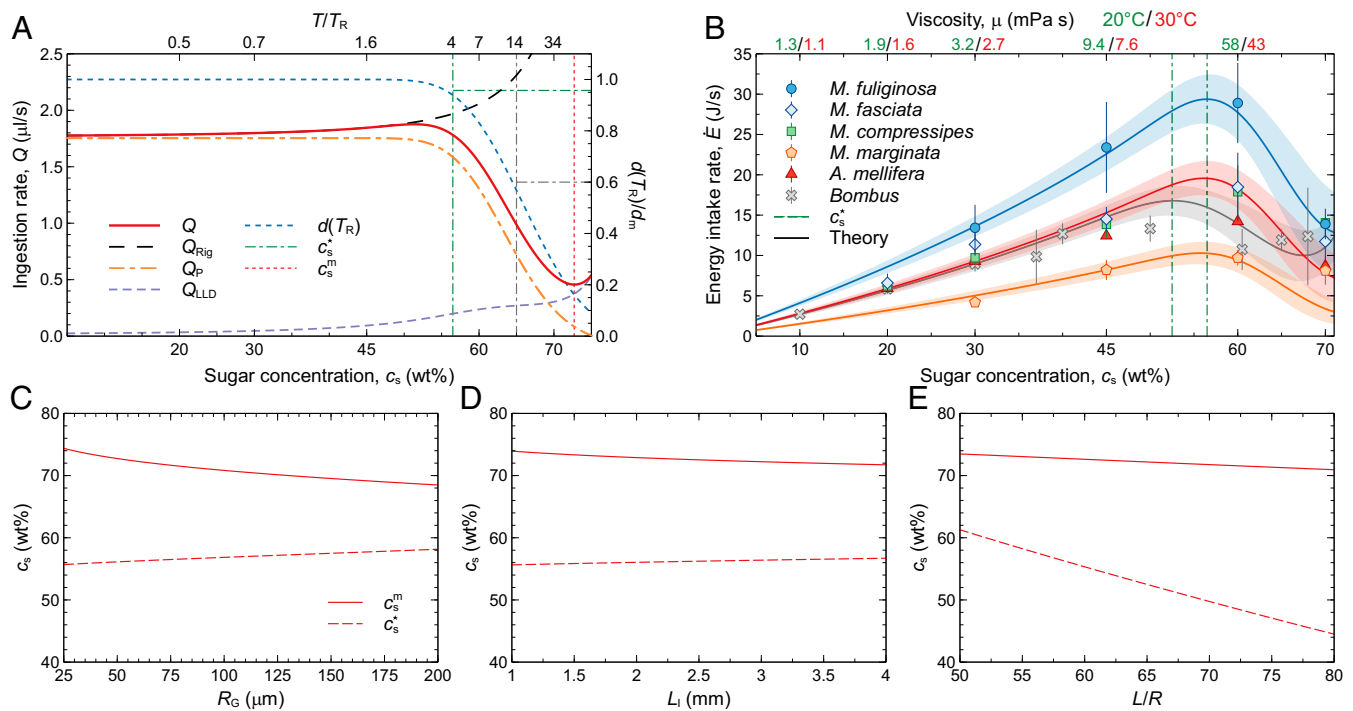


Fig. 4. (A) Evolution of the ingestion rate Q as a function of the sugar concentration for *A. mellifera* as shown in Fig. 1D together with the contribution Q_P of the papillae and of the dragged film, Q_{LLD} . The ingestion rate for rigid papillae, Eq. 12, is shown for comparison. The evolution with the sugar concentration c_s of the normalized distance between the tip of the papillae and the glossa at $t = T_R$ [i.e., $d(T_R)/d_m$] is shown on the right axis. The values of this ratio at the optimal value $c_s = c_s^*$ and at $c_s = 65\%$ are highlighted. The values of the ratio T/T_R at some particular sugar concentrations are shown on the top axis. The value c_s^m of the sugar concentration at which Q is minimum is also shown. (B) Evolution of the energy intake rate, \dot{E} , as a function of the sugar concentration for several bee species obtained from Eqs. 11 and 13 with the same parameter values as those used in Fig. 1D. The shaded areas show the regions spanned by the theoretical curves when the parameters are varied within their error bars. The vertical dashed lines indicate the concentrations at which \dot{E} is maximum for *Melipona*, *Apis*, and *Bombus* species. The symbols represent data obtained by using Eq. 13 together with the in vivo measurements of Q shown in Fig. 1D. (C–E) Evolution of the concentration c_s^m , at which the ingestion rate Q is minimum, and of the concentration c_s^* , at which the energy intake rate \dot{E} is maximum, as a function of the glossa radius, R_G (C), of the immersion length L_I (D), and of the papillae aspect ratio L/R (E). The value of the parameters reported in Fig. 1D for *A. mellifera* are used, and R_G , L_I and L/R are varied separately.

the volume trapped by the papillae and the volume dragged by an LLD mechanism (28–31). The former is delimited by the glossa of radius R_G and the tip of the papillae located at a distance $d(T_R)$ from the glossa (Eq. 10). This volume per unit of time, Q_P , reads $Q_P = \pi v_R [\tilde{R}_G^2 - R_G^2]$, where $\tilde{R}_G = R_G + d(T_R)$ and $v_R = L_I/T_R$ is the average retraction velocity with L_I the immersed length of the tongue. The total volume of the immersed papillae is negligible (SI Appendix). The volume dragged per unit of time by the hairy structure through an LLD mechanism is given by $Q_{LLD} = \pi v_R [(\tilde{R}_G + h)^2 - \tilde{R}_G^2]$, where $h = 1.34 \tilde{R}_G Ca^{2/3}$ is the thickness of the film of nectar dragged (30, 31), $Ca = \mu v_R/\gamma$ is the capillary number, and $\gamma \simeq 0.074$ N/m is the surface tension that does not vary significantly with c_s (46). The total volume of nectar collected per unit of time, $Q = Q_P + Q_{LLD}$, is thus finally given by

$$Q = \pi v_R \left[[R_G + d(T_R)]^2 \left[1 + 1.34 Ca^{2/3} \right]^2 - R_G^2 \right], \quad [11]$$

with $d(T_R)$ given by Eq. 10.

At low c_s , the papillae relaxation time, T , is smaller than the retraction time, T_R , so that $d(T_R) = d_m$. The ingestion rate is then essentially constant, $Q \simeq \pi v_R [(R_G + d_m)^2 - R_G^2]$, in agreement with the in vivo measurements reported in Fig. 1D. The volume captured in this case is thus essentially equal to the volume trapped by the papillae, $Q \simeq Q_P$, since the thickness h of the dragged film is negligible ($Ca \ll 1$). At sufficiently large sugar concentration, $c_s \gtrsim 50\%$, T becomes significantly larger than T_R .

The papillae do not have enough time to fully open, $d(T_R) < d_m$, when the tongue retracts out of nectar, which impacts the ingestion rate (Fig. 4A). Using the measured physiological parameters of *B. terrestris* (Fig. 1D and SI Appendix), Eq. 11 describes well the in vivo data reported in Fig. 1D. A similar quantitative agreement is obtained for *Apis mellifera* when their physiological parameters reported in the literature are used. Fig. 1D reveals also a correlation between the ingestion rate, Q , and the total length of the tongue, L_T (10). Using the values of L_I reported in Fig. 1D while keeping all of the other parameters unchanged, Eq. 11 also describes well the data for *Melipona* species.

Fig. 4A shows that, for moderate sugar concentrations, the volume of the film dragged through an LLD mechanism is negligible compared with the volume trapped by the papillae, whereas it becomes dominant at large c_s . Indeed, the sharp increase in viscosity observed for $c_s \simeq 70\%$ impacts strongly the relaxation dynamics of the papillae, which remain in close contact with the glossa during retraction (i.e., the fine structure of the tongue can no longer help in collecting nectar). Notice that for rigid microstructures mimicking the papillae (12), $d(T_R) = d_m$ for all c_s so that Eq. 11 becomes

$$Q_{Rig} = \pi v_R \left[[R_G + d_m]^2 \left[1 + 1.34 Ca^{2/3} \right]^2 - R_G^2 \right]. \quad [12]$$

Eq. 12 and Fig. 4A show a continuous increase of Q_{Rig} with c_s . The sharp drop observed for Q at large c_s , which is well described by Eq. 11, is therefore a clear signature of the papillae flexibility.

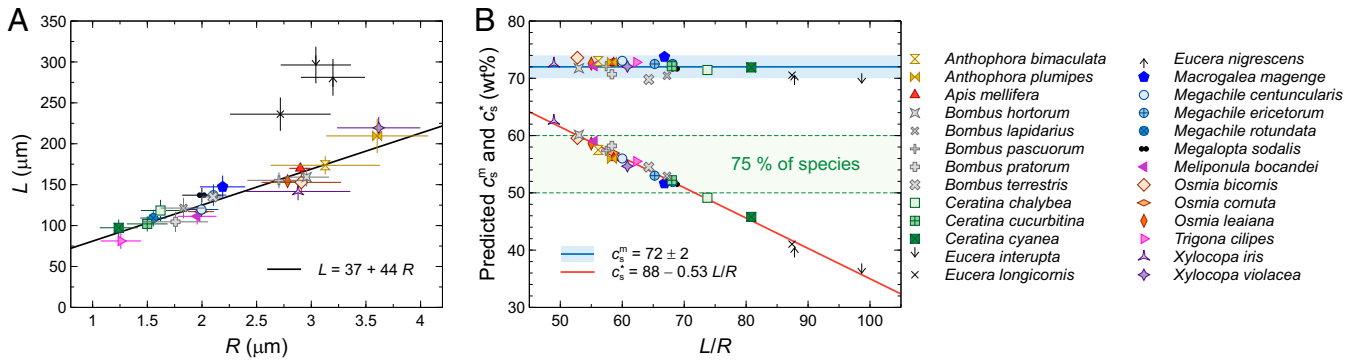


Fig. 5. (A) Evolution of the papillae length L as a function of their radius R for 26 bee species measured on SEM images (SI Appendix, Table S1). The solid line highlights a linear relationship where the coefficients are given for L and R measured in micrometers. (B) Evolution of the sugar concentration c_s^m , at which the ingestion rate Q is minimum, and of the sugar concentration c_s^* , at which the energy intake rate \dot{E} is maximum, as a function of the ratio L/R for the same bee species. These two concentrations have been computed from Eqs. 11 and 13 using the values of R_G , L , and R associated with each species (A and SI Appendix, Table S1) together with the values of T_L , T_R , d_m , E , and ρ_l used in Fig. 1D for all species. Since the influence of L_l on those concentrations is very limited (Fig. 4D) c_s^m and c_s^* are averaged for L_l varying between 1 and 4 mm (SI Appendix, Table S1). c_s^m is essentially constant, whereas c_s^* varies linearly with L/R in good approximation.

After the ingestion rate is known, the energy intake rate, \dot{E} , can be easily computed using

$$\dot{E}(c_s) = \sigma Q(c_s) \rho_l(c_s) c_s, \quad [13]$$

where $\sigma = 15.48$ kJ/g is the energy content per unit mass of sugar (11) and Q is given by Eq. 11. The dependence of the nectar mass density on the sugar concentration is here taken into account (SI Appendix, Eq. S17) since \dot{E} varies linearly with ρ_l in contrast to Q , which depends very weakly on this quantity. Fig. 4B shows that \dot{E} is maximum at $c_s^* \simeq 56\%$ for *Melipona* and *Apis* species and at $c_s^* \simeq 53\%$ for *Bombus* in agreement with values reported previously (11, 14). Fig. 4A shows that the papillae are still open at about 95% of their full erection at those optimal concentrations when the tongue is withdrawn from the nectar [i.e., $d(T_R)/d_m \simeq 0.95$]. However, the ratio $d(T_R)/d_m$ drops quickly above these optimal concentrations. For example, the papillae are only open at 60% when $c_s = 65\%$.

Fig. 4 A and B shows the existence of two characteristic concentrations: c_s^m at which the ingestion rate Q is minimum and c_s^* at which the energy intake rate is maximum. The variations of these concentrations with respect to changes in the tongue morphology can be studied by varying the radius of the glossa R_G , the immersion length L_l , and the papillae aspect ratio L/R in the model. As illustrated in Fig. 4 C–E, the elastoviscous model shows that the concentration c_s^m is rather insensitive to the values of R_G , L_l , and L/R . However, the aspect ratio L/R has a significant impact on the concentration c_s^* , whereas R_G and L_l have a very limited influence. Therefore, the drop in ingestion rate Q appears to be universal and should occur for most bee species at a similar value, close to 70% in sugar concentration, whereas the optimal concentration could vary with the bee species if the ratio L/R is not constant.

To gain a real insight into the possible variation of c_s^m and c_s^* among bees, we have measured R_G , L , and R on scanning electron microscopy (SEM) images for 24 additional long-tongued bee species from different genera distributed in Europe, Africa, and South America (SI Appendix). Fig. 5A shows that L increases linearly with R for all species except the *Eucera* species, which are characterized by more slender papillae. The values of these parameters are then used with Eqs. 10 and 11 to compute c_s^m and c_s^* as a function of the papillae aspect ratio L/R (Fig. 5B). As expected, the value of c_s^m is essentially constant, whereas c_s^* varies linearly with L/R . Such a simple relation can be used

ful to estimate the optimal sugar concentration for various bee species. Nevertheless, since L/R varies between 50 and 70 for most species, the variation of c_s^* is moderate: $c_s^* = (55 \pm 5)\%$ for 75% of the species analyzed. This physiological limit of the bees' tongues may explain why the sugar concentration in nectar offered by flowers rarely exceeds 60% (25, 26). The observed adequacy of the physiological limit for bees and the maximum sugar concentration in flowers' nectar is probably not fortuitous and could be another example of the coevolution of connected species.

The present study explains the role of the papillae in the feeding process for bees. At low sugar concentration, the amount of nectar collected per unit time is essentially constant and controlled by the size of the tongue (i.e., the immersion length L_l and the glossa radius R_G) and by the length L of the papillae. As intuitively expected, larger bees collect more nectar per lap than smaller bees since the proboscis length increases essentially linearly with the body size (47). However, combined in vivo measurements and theoretical model show that the physiological limit for the nectar capture for various bee species is around 70% in sugar concentration. This limit is directly determined by the flexibility of the papillae and its associated relaxation time. Unexpectedly, this parameter discarded in most previous studies finally appears to be a crucial ingredient.

Materials and Methods

B. terrestris from the Biobest firm were used for the in vivo experiments. The colony was kept at the temperature of 27°C and humidity of 65 to 70%. They were fed every 2 d with pollen candies, and a sweet solution imitating the nectar (Biogluc pink) is provided to them ad libitum.

Ingestion Rate. Before beginning the observation of the drinking process, bumblebees were starved at the room temperature in the dark from 12 to 4 h. A bumblebee was then transferred into a centrifuge tube of 15 mL with a 4-mm hole at the tip. After a habituation phase of 3 min, the extension of the proboscis was motivated by presenting a drop of a solution of diluted honey. Finally, a capillary tube with an inner diameter $D_c = 0.8$ mm containing a sweet solution of known sugar concentration (or equivalently, viscosity) was presented to the bumblebee. The inner diameter is similar to the nectar tube width of some plants visited by *Bombus* (48, 49). The experiments were recorded by a camera Logitech C920 at 30 frames per second (Movie S1). The position $p(t)$ of the meniscus at the liquid–air interface was measured as a function of time, and the ingestion rate was obtained from $Q(t) = \pi D_c^2 v_m(t)/4$, where $v_m(t) = dp(t)/dt$ is the velocity of the meniscus. Since $p(t) \sim t$, v_m and Q are constant.

Relaxation Dynamics of Papillae. Bumblebees were starved from 1 to 2 h before beginning the experiment. A bumblebee was then transferred into a centrifuge tube of 50 mL with a 5-mm hole at the tip where it underwent a habituation phase of 3 min. A sweet solution of known viscosity was placed between two microscope slides spaced by a distance of 1 mm and was presented to the bumblebee. The capture dynamics were recorded under a binocular (Leica MZ16) fitted with a Photron Fastcam Mini AX200 operating at 1,000 frames per second with a $1,024 \times 1,024$ -pixel resolution (Movie S1). The distance $x(t)$ between the tip of the tongue and the galea and the distance $d(t)$ between the tip of the papillae and the glossa were measured on each recorded image as detailed in SI Appendix.

Relaxation Dynamics of Rods. Rods made of various materials (steel, polylactide, and polyethylene terephthalate) with length $1.1 \text{ cm} \leq L \leq 9.0 \text{ cm}$, radius $0.15 \text{ mm} \leq R \leq 0.4 \text{ mm}$, Young modulus $5 \text{ GPa} \leq E \leq 165 \text{ GPa}$, and density $1,400 \text{ kg/m}^3 \leq \rho_s \leq 8,300 \text{ kg/m}^3$ were clamped at one extremity and deflected at their free end while immersed in various liquids (water, glycerol, and silicone oil from FungiLab) with viscosity $10^{-3} \text{ Pa s} \leq \mu \leq 10 \text{ Pa s}$ and density $950 \text{ kg/m}^3 \leq \rho_l \leq 1,100 \text{ kg/m}^3$. The size of the fluid container is $32 \times 115 \times 60 \text{ mm}^3$. The bending and Young moduli have been determined from the profile of the rods bent by a known force applied at their free end. The densities of both solids and liquids have been obtained by weighing a known volume of materials.

- P. M. Reis, S. Jung, J. M. Aristoff, R. Stocker, How cats lap: Water uptake by *Felis catus*. *Science* **330**, 1231–1234 (2010).
- A. W. Crompton, C. Musinsk, How dogs lap: Ingestion and intraoral transport in *Canis familiaris*. *Biol. Lett.* **7**, 882–884 (2011).
- W. Kim, J. W. M. Bush, Natural drinking strategies. *J. Fluid Mech.* **705**, 7–25 (2012).
- A. R. Parker, C. R. Lawrence, Water capture by a desert beetle. *Nature* **414**, 33–34 (2001).
- H. W. Krenn, *Insect Mouthparts* (Springer Nature Switzerland AG, Cham, Switzerland, 2019).
- C. D. Michener, *The Bees of the World* (The Johns Hopkins University Press, Baltimore, MD, ed. 2, 2007).
- A. D. Brian, Differences in the flowers visited by four species of bumble-bees and their causes. *J. Anim. Ecol.* **26**, 71–98 (1957).
- I. Teräs, The honeybee's protrusible glossa is a compliant mechanism. *Ann. Zool. Fennici* **13**, 200–232 (1976).
- E. Ranta, H. Lundberg, Resource partitioning in bumblebees: The significance of differences in proboscis length. *Oikos* **35**, 298–302 (1980).
- L. D. Harder, Flower handling efficiency of bumble bees: Morphological aspects of probing time. *Oecologia* **57**, 274–280 (1983).
- L. D. Harder, Effects of nectar concentration and flower depth on flower handling efficiency of bumble bees. *Oecologia* **69**, 309–315 (1986).
- A. Lechante, D. Michez, P. Damman, Collection of nectar by bumblebees: How the physics of fluid demonstrates the prominent role of the tongue's morphology. *Soft Matter* **15**, 6392–6399 (2019).
- L. Shi, S. W. Nicolson, Y. Yang, J. Wu, S. Yan, Z. Wu, Drinking made easier: Honey bee tongues dip faster into warmer and/or less viscous artificial nectar. *J. Exp. Biol.* **223**, jeb229799 (2020).
- D. W. Roubik, S. L. Buchmann, Nectar selection by *Melipona* and *Apis mellifera* (hymenoptera: Apidae) and the ecology of nectar intake by bee colonies in a tropical forest. *Oecologia* **61**, 1–10 (1984).
- C. Zhao, J. Wu, S. Yan, Observations and temporal model of a honeybee's hairy tongue in microfluid transport. *J. Appl. Phys.* **118**, 194701 (2015).
- J. Chen, J. Wu, S. Yan, Switchable wettability of the honeybee's tongue surface regulated by erectable glossal hairs. *J. Insect Sci.* **15**, 164 (2015).
- C.-C. Li, J.-N. Wu, Y.-Q. Yang, R.-G. Zhu, S. Yan, Drag reduction effects facilitated by microridges inside the mouthparts of honeybee workers and drones. *J. Theor. Biol.* **389**, 1–10 (2016).
- R. Zhu, H. Lv, T. Liu, Y. Yang, J. Wu, S. Yan, Feeding kinematics and nectar intake of the honey bee tongue. *J. Insect Behav.* **29**, 325–339 (2016).
- C. Zhao, J. Wu, S. Yan, Erection mechanism of glossal hairs during honeybee feeding. *J. Theor. Biol.* **386**, 62–68 (2015).
- Y. Yang, J. Wu, R. Zhu, C. Li, S. Yan, The honeybee's protrusible glossa is a compliant mechanism. *J. Bionic Eng.* **14**, 607–615 (2017).
- H. Yang, J. Wu, S. Yan, Effects of erectable glossal hairs on a honeybee's nectar-drinking strategy. *Appl. Phys. Lett.* **104**, 263701 (2014).
- H. Peisker, J. Michels, S. N. Gorb, Evidence for a material gradient in the adhesive tarsal setae of the ladybird beetle *Coccinella septempunctata*. *Nat. Commun.* **4**, 1661 (2013).
- S. Gernay, W. Federle, P. Lambert, T. Gilet, Elasto-capillarity in insect fibrillar adhesion. *J. R. Soc. Interface* **13**, 20160371 (2016).
- L. M. Sande, "Materials properties of the lepidopteran proboscis and a bio-inspired characterization method of capillary adhesion," Master's thesis, Clemson University, Clemson, SC (2017).
- G. H. Pyke, N. M. Waser, The production of dilute nectars by hummingbird and honeyeater flowers. *Biotropica* **13**, 260–270 (1981).

The rod was bent by manually displacing its free end by a distance $0.73 \text{ mm} \leq d_m \leq 4.9 \text{ mm}$ depending on the rod length and radius. The initial displacement of the tip of the rod was small with respect to its length, $d_m/L \ll 1$, but large with respect to its radius, $d_m/R \gg 1$. After the free end was released, the motion of the rod was recorded by a Photron Fastcam SA3 high-speed camera operating at 1,000 to 5,000 frames per second until the rod returned to its horizontal equilibrium position. The relaxation dynamics always occur in the plane of the bent rod since recording its motion from different angles did not reveal any lateral deviation of the rod.

Propagation of Uncertainty. The uncertainty, δf , on a quantity $f(x_1, x_2, \dots)$ obtained from the combination of several other quantities x_i with uncertainty δx_i , like Q or T , was computed using the following relation:

$$(\delta f)^2 = \sum_i (\partial f / \partial x_i)^2 (\delta x_i)^2.$$

Data Availability. All study data are included in the article and/or supporting information.

ACKNOWLEDGMENTS. We acknowledge support by Fonds de la Recherche Scientifique Research Grant (Projet de Recherche "ElastoCap") T.0025.19. We thank J. Bico and B. Abou for helping during the in vivo experiments on the papillae relaxation dynamics, P. Flammang and N. Puzozzo for helping during the SEM imaging, and C. Rasmussen for identifying some bee species.

- T. Pamminger, R. Becker, S. Himmelreich, C. W. Schneider, M. Bergtold, The nectar report: Quantitative review of nectar sugar concentrations offered by bee visited flowers in agricultural and non-agricultural landscapes. *PeerJ* **7**, e6329 (2019).
- W. Kim, T. Gilet, J. W. M. Bush, Optimal concentrations in nectar feeding. *Proc. Natl. Acad. Sci. U.S.A.* **108**, 16618–16621 (2011).
- L. Landau, B. Levich, Dragging of a liquid by a moving plate. *Acta Physicochim. URSS* **17**, 42–54 (1942).
- B. V. Derjaguin, On the thickness of the liquid film adhering to the walls of a vessel after emptying. *Acta Physicochim. URSS* **20**, 349–352 (1943).
- B. V. Derjaguin, S. M. Levi, *Film Coating Theory* (The Focal Press, London, United Kingdom, 1964).
- D. Quéré, Fluid coating on a fiber. *Annu. Rev. Fluid Mech.* **31**, 347–384 (1999).
- A. Shimizu et al., Fine-tuned bee-flower coevolutionary state hidden within multiple pollination interactions. *Sci. Rep.* **4**, 3988 (2014).
- J. Wu, R. Zhu, S. Yan, Y. Yang, Erection pattern and section-wise wettability of honeybee glossal hairs in nectar feeding. *J. Exp. Biol.* **218**, 664–667 (2015).
- Y. Zhao, J. Wu, S. Yan, The morphology and reciprocation movement of honeybee's hairy tongue for nectar uptake. *J. Bionic Eng.* **13**, 98–107 (2016).
- Z. He, W. Zhang, Y. Sun, C. Li, J. Wu, Z. Wu, How honey bees dip nectar: Dynamic spacing of tongue hairs facilitates to collect nectar of various viscosities. *J. Theor. Biol.* **512**, 110538 (2021).
- M. Scherge, S. N. Gorb, *Biological Micro- and Nanotribology* (Springer-Verlag, Berlin, Germany, 2001).
- C. Liao et al., Feeding behavior of honey bees on dry sugar. *J. Insect Physiol.* **124**, 104059 (2020).
- L. D. Landau, E. M. Lifshitz, *Theory of Elasticity* (Pergamon Press, New York, NY, ed. 3, 1986).
- F. M. White, *Fluid Mechanics* (McGraw-Hill, New York, NY, ed. 7, 2011).
- H. Lamb, On the uniform motion of a sphere through a viscous fluid. *Lond. Edinb. Dubl. Phil. Mag.* **21**, 112–121 (1911).
- M. Mathlouthi, J. Génotelle, "Rheological properties of sucrose solutions and suspensions" in *Sucrose—Properties and Applications*, M. Mathlouthi, P. Reiser, Eds. (Blackie Academic and Professional, London, United Kingdom, 1995), pp. 126–154.
- R. Saggin, J. N. Coupland, Rheology of xanthan/sucrose mixtures at ultrasonic frequencies. *J. Food Eng.* **65**, 49–53 (2004).
- M. Quintas, T. R. S. Brandão, C. L. M. Silva, R. L. Cunha, Rheology of supersaturated sucrose solutions. *J. Food Eng.* **77**, 844–852 (2006).
- D. Bierman, W. H. Herrmstein, "The interference between struts in various combinations" (Tech. Rep. 468, National Advisory Committee for Aeronautics, Washington, DC, 1933).
- P. W. Bearman, A. J. Wadcock, The interaction between a pair of circular cylinders normal to a stream. *J. Fluid Mech.* **61**, 499–511 (1973).
- V. Aroulmoji, V. Aguié-Béghin, M. Mathlouthi, R. Douillard, Effect of sucrose on the properties of caffeine adsorption layers at the air/solution interface. *J. Colloid Interface Sci.* **276**, 269–276 (2004).
- D. P. Cariveau et al., The allometry of bee proboscis length and its uses in ecology. *PLoS One* **11**, e0151482 (2016).
- S. G. T. Klumpers, M. Stang, P. G. L. Klinkhamer, Foraging efficiency and size matching in a plant–pollinator community: The importance of sugar content and tongue length. *Ecol. Lett.* **22**, 469–479 (2019).
- M. A. Peucker et al., Floral traits are associated with the quality but not quantity of heterospecific stigmatic pollen loads. *BMC Ecol.* **20**, 54 (2020).

Supplementary Information for

Essential role of papillae flexibility in nectar capture by bees

Amandine Lechantre, Ayrton Draux, Hoa-Ai Béatrice Hua, Denis Michez, Pascal Damman, Fabian Brau

Fabian Brau.

E-mail: fabian.brau@ulb.ac.be

This PDF file includes:

Supplementary text
Figs. S1 to S4
Table S1
Legend for Movie S1
Legend for Dataset S1
SI References

Other supplementary materials for this manuscript include the following:

Movie S1
Dataset S1

Supporting Information Text

1. Additional information about materials and methods

Relaxation dynamics of papillae – The distance $x(t)$ between the tip of the tongue and the galea is measured on each recorded image using ImageJ, see Movie S1 and Fig. S1B. The radius R_G of the glossa is measured at four distances from its tip (Fig. S1B,H) where the total width of the tongue, $2(d(t) + R_G)$, is measured on each image. To measure this width, the image at $t = 0$ (Fig. S1A) is subtracted from the image to analyze (Fig. S1B). The contrast of the resulting image is then increased to enhance the signal (Fig. S1C). This procedure avoid losing parts of the signal that could result from a binarization due to the sensible choice of the threshold. Figure S1D shows the superimposition of the contour of Fig. S1C on the image to analyze Fig. S1B. The evolution along a cross-section of the gray value of the enhanced image (Fig. S1C) is shown in Fig. S1E where $d(t)$ can be measured. Finally, the temporal evolution of $x(t)$ and $d(t)$ are shown in Fig. S1F,G. The length of the (bare) flabellum is subtracted from the maximum value x_m of $x(t)$ to obtain the immersion length of the tongue used in the main text, $L_I \simeq 2.0$ mm. The maximum value of $d(t)$ is related to the length of the papillae

by the relation $d_m = L \sin(\pi/4) \simeq 95 \mu\text{m}$ where $L \simeq 135 \mu\text{m}$. The length and radius of the papillae are measured on SEM images.

Figure S1H shows that the radius of the glossa varies slightly along its length according to $R_G(x) = 0.035x + 56$ where R_G and x are expressed in μm . The mean radius over the region where the papillae are located ($x_1 \simeq 120 \mu\text{m}$ and $x_2 \simeq 2120 \mu\text{m}$) is

$$\langle R_G \rangle = \frac{1}{x_2 - x_1} \int_{x_1}^{x_2} R_G(x) dx \simeq 95 \mu\text{m}.$$

This is the value used in the main text for *Bombus*. Similarly, Fig. S1H shows that d_m varies also slightly along the glossa according to $d_m(x) = 0.01x + 83.5$ where d_m and x are expressed in μm . The mean value over the region where the papillae are located is

$$\langle d_m \rangle = \frac{1}{x_2 - x_1} \int_{x_1}^{x_2} d_m(x) dx \simeq 95 \mu\text{m}.$$

This is the value used in the main text for *Bombus* through the relation $d_m = L \sin(\pi/4)$ with $L \simeq 135 \mu\text{m}$.

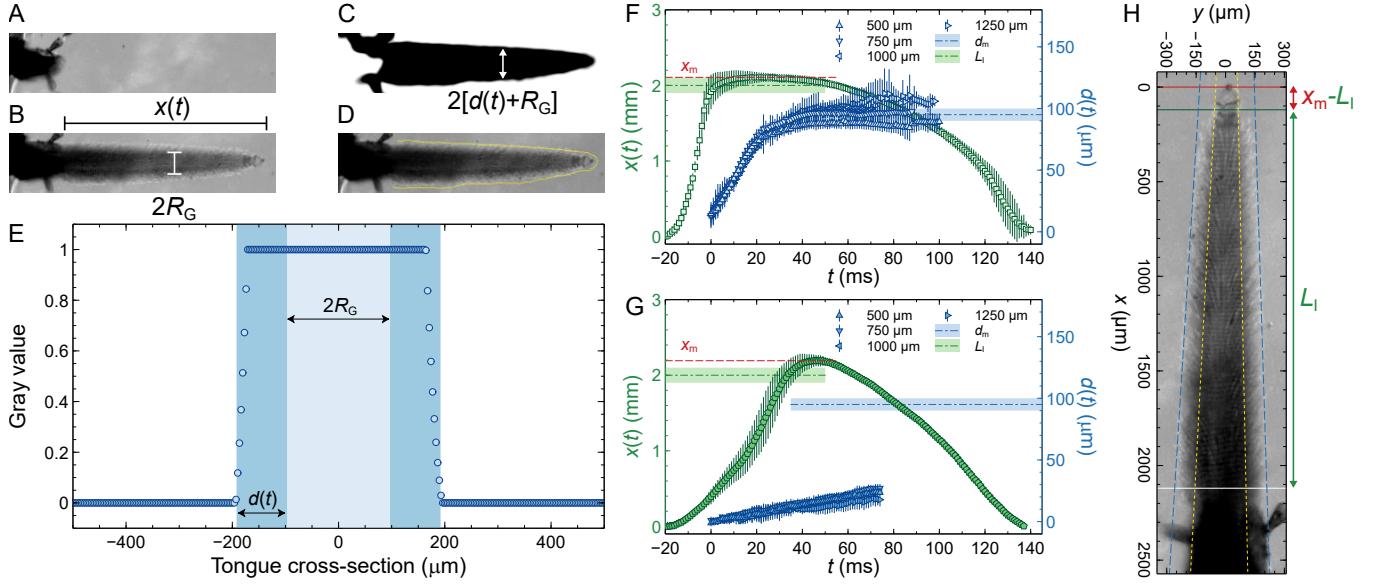


Fig. S1. (A)-(E) Measurements of the distance $x(t)$ between the tip of the tongue and the galea and of the distance $d(t)$ between the tip of the papillae and the glossa of radius R_G . The image at $t = 0$ (A) is subtracted from the image to analyse (B) and the contrast is increased to obtain the image (C). The image (D) shows the contour of image (C) superimposed on image (B). The distance $x(t)$ and the radius R_G of the glossa are measured on image (B) with ImageJ. The total width of the tongue is measured on image (C) at given distances from the tongue tip. (E) Evolution of the grayscale value of the image (C) along a cross-section shown by the double arrow. (F) Temporal evolution of the distance $x(t)$ between the tip of the tongue and the galea (green symbols) and of the distance $d(t)$ between the tip of the papillae and the glossa (blue symbols) averaged over 10 cycles for $c_s = 37\%$ ($\mu = 5$ mPa s). $d(t)$ is measured at four distances from the tip of the tongue as indicated. The average of these data are displayed in Fig. 2C of the main text. (G) Same as panel (F) for $c_s = 66\%$ ($\mu = 200$ mPa s) and averaged over 3 cycles. (H) Snapshot for $c_s = 37\%$ taken 63 ms after the protraction started so that the tongue is essentially fully extended and the papillae fully opened. The equations of the yellow dotted lines are $R_G^+ = 0.02x + 62$ and $R_G^- = -0.05x - 50$ and the variation of the glossa radius along its length is $R_G = (R_G^+ - R_G^-)/2 = 0.035x + 56$ for $x \in [120, 2120]$. The equations of the blue dashed lines are $w^+ = 0.03x + 147$ and $w^- = -0.06x - 132$ so that the variation of the total width along the glossa length is $w = (w^+ - w^-) = 0.09x + 279$. The variation of d_m along the glossa is $d_m = (w - 2R_G)/2 = 0.01x + 83.5$.

2. Additional information about the model

A. Total volume of the immersed papillae. In the capture model presented in the main text, the total volume of the immersed papillae are neglected. Indeed, according to Refs. (1–6), the number of papillae per unit area is $2500/\text{mm}^2$ for *Apis mellifera*. The area of the immersed part of the tongue is $A \simeq 2\pi R_G L_I$. Using $R_G = 50 \mu\text{m}$ and $L_I = 2.2$ mm, the number of immersed papillae is $N \simeq 1728$. The total volume of the papillae is thus $\pi R^2 L N = 7.8 \times 10^{-3} \mu\text{L}$ which is negligible compared to the volume per lap $QT_L \simeq 1.8 \mu\text{L}/\text{s} \times 0.2 \text{ s} \simeq 0.36 \mu\text{L}$.

B. Order of magnitude of the papillae's Young modulus. Figure 2B of the main text shows that the capillary forces are strong enough to fully bend the papillae. This implies that the length L of the papillae is such that $L \gg L_{BC}$ where $L_{BC} = [B/\gamma R]^2$ is the bendocapillary length, B the bending modulus of the papillae, R their radius and γ the surface tension of the liquid (7). In addition, the papillae sustain their own weight. This implies that $L \ll L_g$ where $L_g = [B/\rho_s g S]^2$ is the elasto-gravitational length, ρ_s the mass density of the papillae, g the gravitational acceleration and S the cross section area of the papillae (8). Using the parameter values reported in Fig. 1D of the main text together with $\rho_s \simeq 10^3 \text{ kg/m}^3$ and $\gamma \simeq 0.07 \text{ N/m}$, these two inequalities yield $10^{-2} \text{ MPa} \ll E \ll 10^2 \text{ MPa}$ in agreement with the value of E reported in the caption of Fig. 1D of the main text.

C. Linear viscous force. In the main text, we have approximated the viscous force by a power law, see Eq. [5], whose

exponent is close to 1. We study here the impact of an additional approximation where the viscous force behaves linearly with the rod velocity. Figure 3C of the main text shows that we have approximately

$$\bar{F}_\mu = S_g \bar{\beta} \bar{v}, \quad \bar{\beta} = 0.1. \quad [1]$$

In the overdamped regime, the rod inertia is negligible and, since there is no oscillations, the rod velocity is negative such that $|\partial_{\bar{t}} \bar{w}| = -\partial_{\bar{t}} \bar{w}$ and $S_g = -1$. Therefore, Eq. [4] of the main text with the viscous force [1] becomes

$$k \partial_{\bar{x}}^4 \bar{w}(\bar{x}, \bar{t}) = \bar{\beta} [-\partial_{\bar{t}} \bar{w}(\bar{x}, \bar{t})]. \quad [2]$$

Using the separation of variables, $\bar{w}(\bar{x}, \bar{t}) = \bar{w}_E(\bar{t})g(\bar{x})$ where $\bar{w}_E(\bar{t})$ describes the temporal evolution of the tip of the rod, Eq. [2] reduces to two ODEs

$$\dot{\bar{w}}_E = -\frac{\eta k}{\bar{\beta}} \bar{w}_E, \quad \bar{w}_E(0) = \bar{d}_m, \quad [3a]$$

$$g'''' = \eta g, \quad g(0) = g'(0) = g''(1) = g'''(1) = 0, \quad [3b]$$

where η is the separation constant, $d_m = \ell \bar{d}_m$ is the imposed transverse displacement of the tip of the rod and dot and prime indicate time and spatial derivative, respectively. The boundary conditions indicate that the rod is clamped at $\bar{x} = 0$ and free at $\bar{x} = 1$. The linear eigenvalue equation [3b] can be solved exactly with $g(1) = 1$, i.e. $\bar{w}(1, 0) = \bar{d}_m$, so that $\eta \simeq 12.362$ (the smallest root of $1 + \cos(\eta^{1/4}) \cosh(\eta^{1/4})$). The temporal evolution of the position of the tip of the rod is then

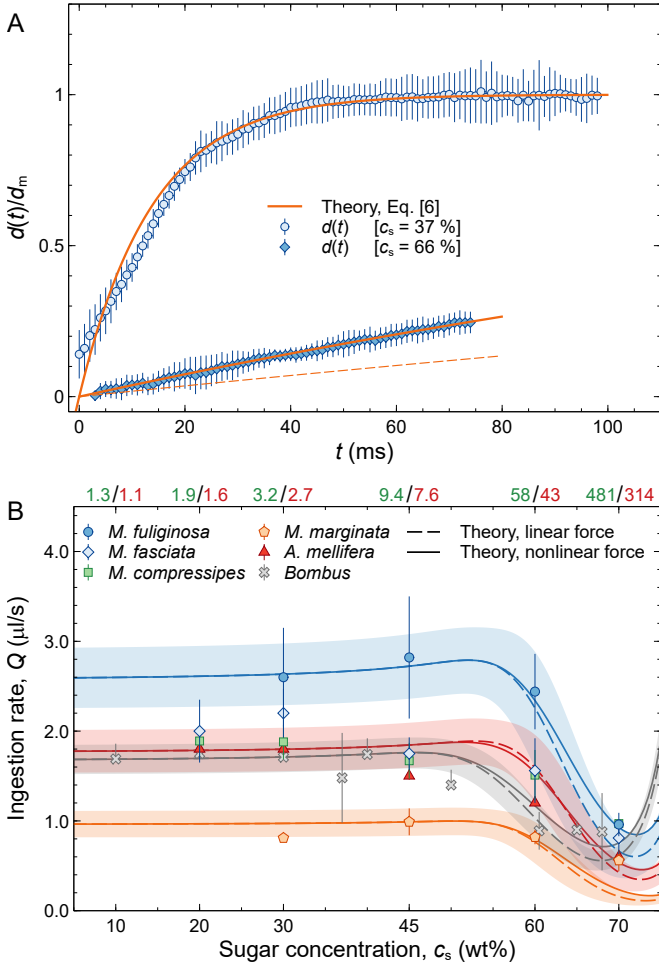


Fig. S2. (A) Evolution of the rescaled distance $d(t)/d_m$ between the tip of the papillae and the glossa as a function of time for two values of c_s for *Bombus terrestris*. The theoretical curves [6] are shown with $\rho_l = 1150 \text{ kg/m}^3$ and $\mu = 5$ and 200 mPa s (20°C) together with R , L , d_m used in Fig. 1D of the main text for *Bombus*. $E = 0.8 \text{ MPa}$ for $c_s = 37\%$ and $E = 1.7 \text{ MPa}$ for $c_s = 66\%$. The dashed orange line is obtained with $E = 0.8 \text{ MPa}$ at $c_s = 66\%$. (B) See caption Fig. 1D of the main text. All the parameter values used to compute Q are the same than in the main text except $E = (1.25 \pm 0.45) \text{ MPa}$ for all species. The dashed lines show the theoretical curves for Q (Eq. [11] of the main text) obtained with $d(T_R)$ given by Eq. [6] (linear viscous force) whereas the solid lines are those shown in Fig. 1D of the main text and obtained with $d(T_R)$ given by Eq. [10] of the main text (nonlinear viscous force).

obtained by integrating Eq. [3a]:

$$\frac{\bar{w}_E(\bar{t})}{\bar{d}_m} = \exp[-(k\eta/\bar{\beta})\bar{t}] = \exp[-11\bar{t}/T], \quad [4]$$

$$\text{where } T = \frac{11\bar{\beta}\tau}{k\eta} = 1.42\frac{\mu}{\bar{E}}, \quad [5]$$

and where $\bar{E} = ER^4/L^4$ as in the main text. Notice that we have introduced the factor 11 in the definition of T so that it has the same meaning than in the main text since in both cases $\dot{w}_E(0) = -11d_m/T$.

The temporal evolution of the distance $d(t) = d_m - w_E(t)$ between the tip of the papillae and the glossa is thus obtained from Eq. [4]

$$\frac{d(t)}{d_m} = 1 - \exp[-11t/T], \quad T = 1.42\frac{\mu}{E}. \quad [6]$$

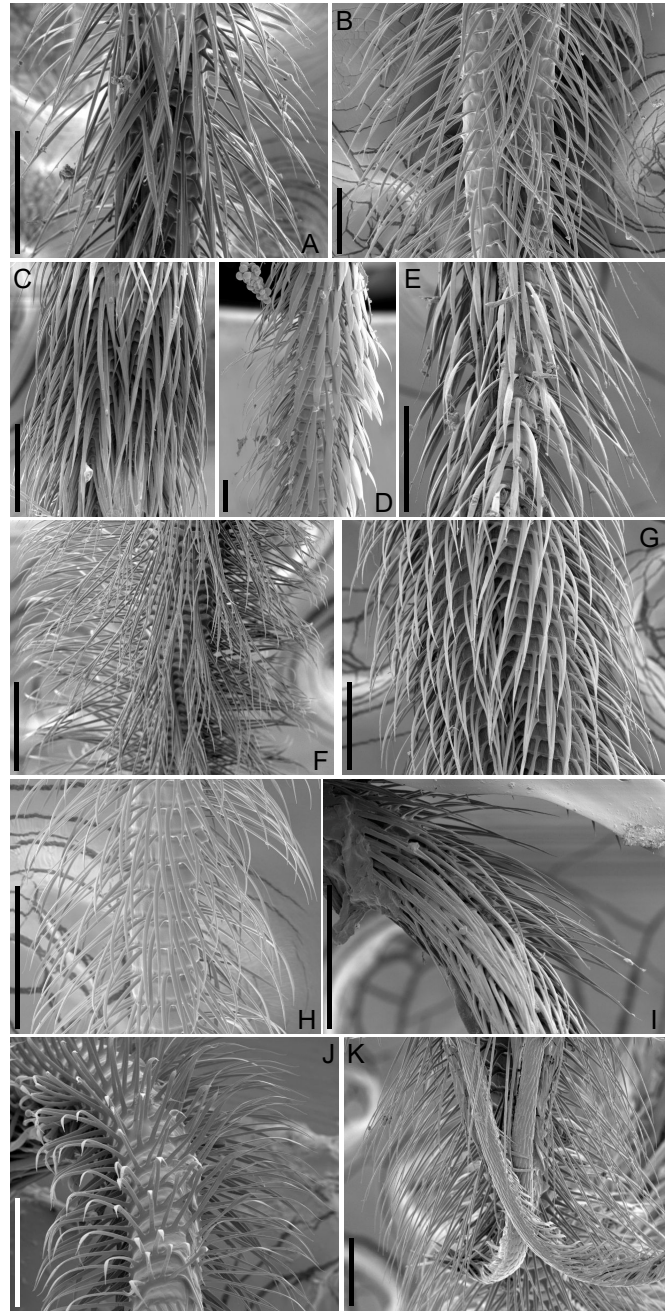


Fig. S3. Representative SEM images of some bee species. (A) *Ceratina chalybea*. (B) *Xylocopa violacea*. (C) *Meliponula bocandei*. (D) *Anthophora plumipes*. (E) *Macrogalea magenge*. (F) *Megalopta sodalis*. (G) *Bombus lapidarius*. (H) *Megachile rotundata*. (I) *Trigona cilipes*. (J) *Osmia cornuta*. (K) *Eucera longicornis*. Scale bars: $100 \mu\text{m}$.

Using the parameter values reported in Fig. 1D of the main text for *Bombus*, the temporal evolution of $d(t)/d_m$ is found to be in good quantitative agreement with *in vivo* measurements of the papillae relaxation dynamics, see Fig. S2A, provided E is allowed to vary over a slightly larger interval compared to the results reported in the main text.

The evolution of the ingestion rate Q with the sugar concentration is now obtained by using Eq. [6] at $t = T_R$ in Eq. [11] of the main text. Figure S2B shows that a good agreement can also be obtained by using a linear viscous force instead a

nonlinear one (even if the model with a linear viscous force yields a smaller value for the minimum of Q). The difference between the two descriptions is smaller than the typical uncertainty on the *in vivo* data. This illustrates further that the important ingredient to describe the evolution of Q with c_s is the flexibility of the papillae and their associated relaxation dynamics and not the small details of this dynamics.

D. Conical papillae and Young modulus. In the study reported in the main text, we take into account the fine structure of the tongue, namely the papillae, to propose a model of nectar capture by bees describing the role of the papillae in the feeding process and able to describe the drop of the ingestion rate observed at large sugar concentrations. In this section, we go one step further by considering the fine structure of the papillae themselves which are conical in good approximation. We show here that it leads to an estimation of E one order of magnitude larger than in the main text. Taking this new value of E into account together with the conical shape of the papillae, all the discussions and results of the main text remain however unchanged.

Equation [1] of the main text can be easily generalized to a rod with a variable cross-section (9):

$$\bar{\rho}_{s1}(x) \partial_t^2 w(x, t) = -\partial_x^2 [B(x) \partial_x^2 w(x, t)] - F_\mu, \quad [7]$$

where $B = EI(x)$, $\bar{\rho}_{s1}(x) = \rho_{s1}S(x)$ and $I(x)$ and $S(x)$ are the variable area moment of inertia and section of the rod, respectively. For a conical rod, we have

$$I(x) = \frac{\pi}{4} R^4 \left[1 - \frac{x}{L} \left(1 - \frac{r}{R}\right)\right]^4 = \frac{\pi}{4} R^4 \bar{I}(x), \quad [8a]$$

$$S(x) = \pi R^2 \left[1 - \frac{x}{L} \left(1 - \frac{r}{R}\right)\right]^2 = \pi R^2 [\bar{I}(x)]^{1/2}, \quad [8b]$$

where R is the radius of the base of the papillae ($x = 0$) and r the radius of their tip ($x = L$). When $r = R$, we recover the expressions for a cylindrical rod.

Using the expression [5] of the main text for the viscous force together with $\bar{w} = w/\ell$, $\bar{x} = x/L$, $\bar{t} = t/\tau$ where ℓ and τ are given by Eq. [3] of the main text, Eq. [7] becomes

$$[\bar{I}(\bar{x})]^{1/2} \partial_{\bar{t}}^2 \bar{w} = -k \partial_{\bar{x}}^2 [\bar{I}(\bar{x}) \partial_{\bar{x}}^2 \bar{w}] - \beta S_g |\partial_{\bar{t}} \bar{w}|^{11/10}, \quad [9a]$$

$$\bar{I}(\bar{x}) = \left[1 - \bar{x} \left(1 - \frac{r}{R}\right)\right]^4, \quad [9b]$$

where k is given by Eq. [4] of the main text.

In the overdamped regime, the rod inertia is negligible and, since there is no oscillations, the rod velocity is negative such that $|\partial_{\bar{t}} \bar{w}| = -\partial_{\bar{t}} \bar{w}$ and $S_g = -1$. Eq. [9a] becomes

$$k \partial_{\bar{x}}^2 [\bar{I}(\bar{x}) \partial_{\bar{x}}^2 \bar{w}(\bar{x}, \bar{t})] = \beta [-\partial_{\bar{t}} \bar{w}(\bar{x}, \bar{t})]^{11/10}. \quad [10]$$

Using the separation of variables, $\bar{w}(\bar{x}, \bar{t}) = \bar{w}_E(\bar{t}) g(\bar{x})$, the nonlinear PDE [10] reduces to two ODEs

$$\dot{\bar{w}}_E = -[\bar{\eta} k/\beta]^{10/11} \bar{w}_E^{10/11}, \quad \bar{w}_E(0) = \bar{d}_m \quad [11a]$$

$$[\bar{I} g'''] = \bar{\eta} g^{11/10}, \quad g(0) = g'(0) = g''(1) = g'''(1) = 0, \quad [11b]$$

where $\bar{\eta}$ is the separation constant, $d_m = \ell \bar{d}_m$ is the imposed transverse displacement of the tip of the rod and dot and prime indicate time and spatial derivative, respectively. The boundary conditions indicate that the rod is clamped at $\bar{x} = 0$ and free at $\bar{x} = 1$. The nonlinear eigenvalue equation [11b]

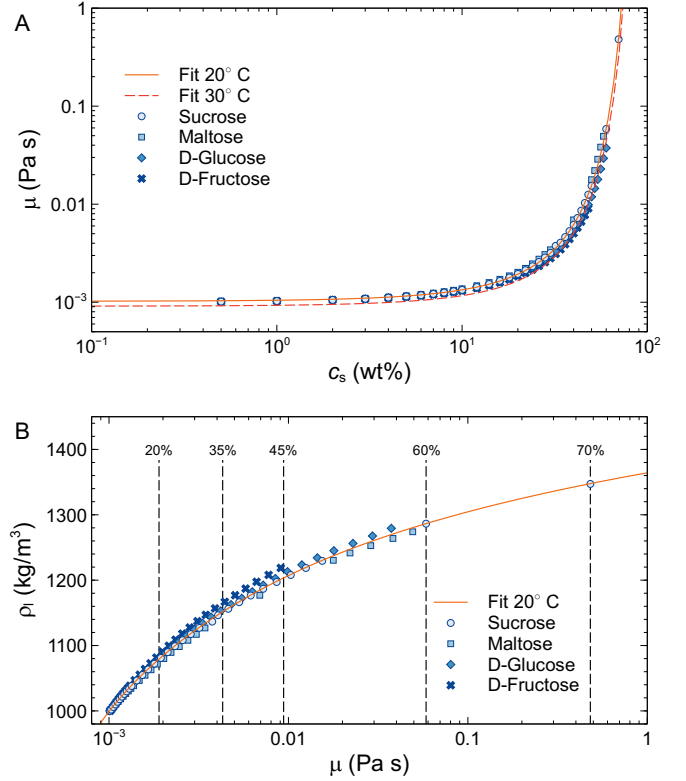


Fig. S4. (A) Viscosity of sugar solutions as a function of the sugar concentration at 20°C (10, ch.8) together with the fit Eq. [15]. The fit at 30°C is shown for comparison. (B) Density of sugar solutions as a function of the viscosity (10, ch.8).

can be solved numerically since, at $\bar{t} = 0$, $\bar{w}(1, 0) = \bar{d}_m = \bar{w}_E(0) g(1)$ so that $g(1) = 1$. Using for example $r/R = 10^{-2}$, we obtain $\bar{\eta} \simeq 1.490$. The nonlinear equation [11a] is then integrated and yields the position of the tip of the rod as a function of time:

$$\frac{\bar{w}_E(\bar{t})}{\bar{d}_m} = \left[1 - 0.405 \frac{k^{10/11}}{\bar{d}_m^{1/11}} \bar{t}\right]^{11}. \quad [12]$$

The relaxation time corresponding to $w_E = 0$ can be computed from Eq. [12] and reads,

$$T/\tau = 2.47 \bar{d}_m^{1/11} k^{-10/11}, \quad [13]$$

which can be written as

$$T = 30.7 \left[\frac{\mu^{10} d_m}{\bar{E}^{10} v_c}\right]^{1/11}, \quad [14]$$

where $\bar{E} = ER^4/L^4$ and $v_c = 4\mu/\rho_1 R$. This is exactly the same expression than Eq. [10] of the main text except for the numerical coefficient which is roughly 7.06 times larger. Therefore, if E is 7.06^{11/10} times larger, i.e. $E \simeq 9.4$ MPa, the relaxation time remains unchanged as well as all the results presented in the main text. If $r/R = 10^{-3}$, the numerical coefficient of Eq. [14] becomes 41.8 and $E \simeq 13.3$ MPa.

3. Tongue morphology of various bee species

The elasto-viscous model proposed in the main text shows that the concentration c_s^m at which the ingestion rate Q is minimum is rather insensitive to the values of the tongue

Species	L (μm) [N]	R (μm) [N]	R_G (μm)	c_s^m (wt%)	c_s^* (wt%)
<i>Anthophora bimaculata</i>	174 \pm 11 [27]	3.1 \pm 0.5 [25]	53 \pm 2	74.1 – 71.9	56.9 – 58.1
<i>Anthophora plumipes</i>	210 \pm 21 [22]	3.6 \pm 0.5 [61]	62 \pm 10	73.9 – 71.7	55.4 – 56.5
<i>Bombus hortorum</i>	159 \pm 12 [19]	3.0 \pm 0.2 [20]	91 \pm 8	73.1 – 70.4	59.2 – 61.1
<i>Bombus lapidarius</i>	121 \pm 12 [39]	1.8 \pm 0.2 [65]	61 \pm 15	71.8 – 69.1	52.4 – 53.5
<i>Bombus pascuorum</i>	155 \pm 10 [26]	2.7 \pm 0.3 [34]	65 \pm 16	73.3 – 70.9	56.7 – 58.0
<i>Bombus pratorum</i>	105 \pm 12 [21]	1.8 \pm 0.3 [50]	70 \pm 3	72.1 – 69.3	57.3 – 59.1
<i>Ceratina chalybea</i>	118 \pm 13 [28]	1.6 \pm 0.2 [53]	32 \pm 2	72.6 – 70.3	48.8 – 49.5
<i>Ceratina cucurbitina</i>	102 \pm 9 [15]	1.5 \pm 0.2 [25]	28 \pm 2	73.2 – 71.0	51.8 – 52.6
<i>Ceratina cyanea</i>	97 \pm 10 [67]	1.2 \pm 0.2 [61]	17 \pm 2	73.0 – 70.8	45.5 – 46.1
<i>Eucera interrupta</i>	296 \pm 22 [18]	3.0 \pm 0.3 [65]	60 \pm 9	70.5 – 67.9	35.8 – 36.2
<i>Eucera longicornis</i>	236 \pm 20 [46]	2.7 \pm 0.5 [39]	46 \pm 4	71.7 – 69.4	40.8 – 41.3
<i>Eucera nigrescens</i>	281 \pm 22 [30]	3.2 \pm 0.3 [30]	53 \pm 9	71.7 – 69.3	40.2 – 40.6
<i>Macrogalea magenge</i>	147 \pm 14 [27]	2.2 \pm 0.2 [24]	20 \pm 1	74.7 – 72.8	51.3 – 52.0
<i>Megachile centuncularis</i>	120 \pm 9 [47]	2.0 \pm 0.2 [65]	32 \pm 4	74.1 – 72.0	55.5 – 56.5
<i>Megachile ericetorum</i>	137 \pm 13 [29]	2.1 \pm 0.1 [39]	35 \pm 4	73.6 – 71.4	52.6 – 53.4
<i>Megachile rotundata</i>	109 \pm 10 [75]	1.6 \pm 0.1 [96]	25 \pm 3	73.6 – 71.4	51.5 – 52.3
<i>Megalopta sodalis</i>	137 \pm 9 [42]	2.0 \pm 0.2 [23]	42 \pm 10	72.8 – 70.5	51.1 – 51.9
<i>Meliponula bocandei</i>	111 \pm 10 [11]	2.0 \pm 0.2 [25]	51 \pm 1	73.4 – 70.9	58.3 – 59.8
<i>Osmia bicornis</i>	153 \pm 14 [15]	2.9 \pm 0.4 [47]	45 \pm 13	74.7 – 72.5	58.9 – 60.2
<i>Osmia cornuta</i>	117 \pm 7 [30]	2.0 \pm 0.1 [38]	35 \pm 1	74.0 – 71.8	56.4 – 57.5
<i>Osmia leaiana</i>	154 \pm 3 [3]	2.8 \pm 0.1 [3]	61 \pm 15	73.7 – 71.4	57.9 – 59.3
<i>Trigona cilipes</i>	81 \pm 10 [28]	1.3 \pm 0.2 [44]	23 \pm 3	73.9 – 71.7	55.0 – 56.0
<i>Xylocopa iris</i>	142 \pm 11 [26]	2.9 \pm 0.5 [79]	73 \pm 22	73.9 – 71.2	61.5 – 63.6
<i>Xylocopa violacea</i>	219 \pm 13 [65]	3.6 \pm 0.4 [42]	76 \pm 17	73.2 – 70.9	54.1 – 55.2

Table S1. Physiological parameters of the tongue of 24 bee species. N indicates the number of papillae analyzed. The error on L and R comes from the averaging over N whereas the error on R_G reflects its variation over the glossa length visible on the SEM images. The radius R has been measured near the base of the papillae. The values of c_s^m and c_s^* have been computed from Eqs. [11] and [13] of the main text using the values of R_G , L and R associated with each species together with the values of T_L , T_R , d_m , E and ρ_1 used in Fig. 1D of the main text for all species. The range of values of c_s^m and c_s^* is obtained by varying the immersion length L_I from 1 to 4 mm. The impact of this parameter on these concentrations is seen to be small as expected from the results shown in Fig. 4D of the main text.

radius R_G , of the immersion length L_I and of the papillae aspect ratio L/R , see Fig. 4C-E of the main text. Therefore, this concentration should be quite universal and valid for most bees. The model shows also that the concentration c_s^* at which the energy intake rate \dot{E} is maximum varies more significantly with L/R whereas it is also rather insensitive to the values of R_G and L_I . Therefore, the optimal concentration c_s^* could vary with the bee species if the ratio L/R is not constant.

We have therefore measured R_G , L and R for 24 additional bee species. Figure S3 shows representative SEM images on which those lengths have been measured and their values are gathered in Table S1. Figure 5A of the main text shows that the length of the papillae increases linearly with their radius (except for the *Eucera* species). Figure 5B of the main text shows that the ratio L/R is not constant and varies between 50 and 70 for most species considered in this work. Therefore, c_s^* slightly varies among species and evolves linearly with L/R . Nevertheless, its variation is limited since it ranges between 50 and 60% for most species. However, as expected, c_s^m is essentially constant for all species.

4. Sugar solution viscosity and density

Figure S4A shows the evolution of the viscosity of various sugar solutions as a function of the sugar concentration at 20°C (10, ch.8). The data are nicely fitted using the following expression adapted from Ref. (11)

$$\mu_{20^\circ}(x) = (976.27)^{-1} 10^{0.9652x/(1-x)} 10^{0.8572x^2}, \quad [15]$$

where $x = c_s/100 \in [0, 1]$ is the sucrose concentration (wt%) and μ is the viscosity in Pa s. The numerical coefficients have

been determined using the sucrose data but slight modifications allow to fit the other types of sugar. The viscosity changes slightly with the temperature and at 30°C, we have (11)

$$\mu_{30^\circ}(x) = (1097)^{-1} 10^{0.8752x/(1-x)} 10^{1.01x^2}. \quad [16]$$

Figure S4B shows the evolution of the density of various sugar solutions as a function of their viscosity (10, ch.8). The data are also nicely fitted using the following expression

$$\rho_1 = 1134 \left[\ln \left(\frac{\mu + 0.00132}{0.00175} \right) \right]^{1/10}. \quad [17]$$

Again, the numerical coefficients have been determined using the sucrose data but slight modifications allow to fit the other types of sugar.

Movie S1. Typical experiments performed to measure the ingestion rate and the papillae relaxation dynamics at various sugar concentrations.

SI Dataset S1 (Dataset_S1.xlsx)

The attached data set contains data for the experiments and *in vivo* measurements presented in the main text. Dataset S1A contains data for the evolution of the position $p(t)$ of the liquid-air interface as a function of time (Fig. 1B of the main text). Dataset S1B contains data for the lapping rate as a function of the sugar concentration (Fig. 1C of the main text). Dataset S1C contains data for the variation of the ingestion rate Q as a function of the sugar concentration (Fig. 1D of the main text). Dataset S1D contains data for the distributions of the

volumes per lap associated to the advances and recoils of the meniscus (Fig. 1E,F of the main text). Dataset S1E contains data for the relaxations dynamics of the papillae (Fig. 2C of the main text and Fig. S1F,G). Dataset S1F contains data for the evolution of the experimental rescaled relaxation time T/τ as a function of the control parameter k (Fig. 3B of the main text). Dataset S1G contains data for the evolution of the energy intake rate, \dot{E} , as a function of the sugar concentration (Fig. 4B of the main text). Dataset S1H contains data shown in Table S1.

References

1. H Yang, J Wu, S Yan, Effects of erectable glossal hairs on a honeybee's nectar-drinking strategy. *Appl. Phys. Lett.* **104**, 263701 (2014).
2. C Zhao, J Wu, S Yan, Erection mechanism of glossal hairs during honeybee feeding. *J. Theor. Biol.* **386**, 62–68 (2015).
3. C Zhao, J Wu, S Yan, Observations and temporal model of a honeybee's hairy tongue in microfluid transport. *J. Appl. Phys.* **118**, 194701 (2015).
4. J Wu, R Zhu, S Yan, Y Yang, Erection pattern and section-wise wettability of honeybee glossal hairs in nectar feeding. *J. Exp. Biol.* **218**, 664–667 (2015).
5. CC Li, JN Wu, YQ Yang, RG Zhu, S Yan, Drag reduction effects facilitated by microridges inside the mouthparts of honeybee workers and drones. *J. Theor. Biol.* **389**, 1–10 (2016).
6. Y Zhao, J Wu, S Yan, The morphology and reciprocation movement of honeybee's hairy tongue for nectar uptake. *J. Bionic Eng.* **13**, 98–107 (2016).
7. S Neukirch, B Roman, B de Gaudemaris, B J., Piercing a liquid surface with an elastic rod: Buckling under capillary forces. *J. Mech. Phys. Solids* **55**, 1212–1235 (2007).
8. D Vella, A Boudaoud, M Adda-Bedia, Statics and inertial dynamics of a ruck in a rug. *Phys. Rev. Lett.* **103**, 174301 (2009).
9. LD Landau, EM Lifshitz, *Theory of Elasticity*. (Pergamon Press, New-York), 3 edition, (1986).
10. DR Lide, ed., Concentrative properties of aqueous solutions: density, refractive index, freezing point depression, and viscosity in *CRC Handbook of Chemistry and Physics*. (CRC Press/Taylor and Francis, Boca Raton), 90 edition, pp. 52–77 (2010).
11. KA Pivnick, JN McNeil, Effects of nectar concentration on butterfly feeding: Measured feeding rates for *Thymelicus lineola* (Lepidoptera: Hesperidae) and a general feeding model for adult lepidoptera. *Oecologia* **66**, 226–237 (1985).